Showcasing research from Sergey Koroidov et al. at Stockholm University, Sweden.

Chemisorbed oxygen or surface oxides steer the selectivity in Pd electrocatalytic propene oxidation observed by *operando* Pd L-edge X-ray absorption spectroscopy

Electrochemical propene oxidation on Pd leads to the formation of several high-value and industrially relevant products. In situ Pd L-edge XAS provides insight on the catalytic mechanism and shows the impact the surface oxide formation has on the reaction selectivity.

As featured in:

See Sergey Koroidov, Anders Nilsson *et al.*, *Catal. Sci. Technol.*, 2021, **11**, 3347.

ROYAL SOCIETY OF CHEMISTRY

rsc.li/catalysis

PAPER

Check for updates

Chemisorbed oxygen or surface oxides steer the selectivity in Pd electrocatalytic propene oxidation observed by *operando* Pd L-edge X-ray absorption spectroscopy†

Sergey Koroidov, [iD] *[a] Anna Winiwarter, [iD] ‡[b] Oscar Diaz-Morales, [iD] §[a] Mikaela Görlin, [iD] ¶[a] Joakim Halldin Stenlid, [iD] ||[a] Hsin-Yi Wang, [iD] [a] Mia Börner,[a] Christopher Matthew Goodwin,[a] Markus Soldemo, [iD] [a] Lars Gunnar Moody Pettersson,[a] Jan Rossmeisl, [iD] [c] Tony Hansson,[a] Ib Chorkendorff [iD] [b] and Anders Nilsson [iD] *[a]

Controlled electrochemical oxidation of hydrocarbons to desired products is an attractive approach in catalysis. Here we study the electrochemical propene oxidation under *operando* conditions using Pd L-edge X-ray absorption spectroscopy (XAS) as a sensitive probe to elucidate surface processes occurring during catalysis. Together with *ab initio* multiple-scattering calculations, our XAS results enable assignment of characteristic changes of the Pd L-edge intensity and energy position in terms of a mechanistic understanding of the selective oxidation of propene. The results, supported by electrochemical density functional theory DFT simulations, show that in the potential range of 0.8–1.0 V *vs.* the reversible hydrogen electrode (RHE), selective oxidation of propene to acrolein and acrylic acid occurs on the metallic Pd surface. These reactions are proposed to proceed *via* the Langmuir–Hinshelwood mechanism. In contrast, for the potential range of 1.1–1.3 V *vs.* RHE, selective oxidation of propene to propylene glycol takes place on a Pd oxide surface.

Introduction

Hydrocarbon (HC) oxidation reactions are vital processes in many chemical syntheses. They are mainly performed using thermal heterogeneous catalysis, where the free energy to power the catalytic reaction is provided by elevated temperatures and/or pressures.[1,2] In contrast, in an electrochemical HC oxidation process, the catalytic reaction can be precisely controlled by the applied electrochemical potential allowing for milder reaction conditions. The electrochemical approach also provides the ability to selectively tune the potential to generate a specific product. The potential control can further be used to avoid the full oxidation of the HCs into CO_2 and water, which always are the thermodynamically favoured reaction products under oxidising conditions. Thereby, electrochemical oxidation offers an attractive alternative to traditional industrial production processes as it eliminates the need for the aggressive organic peroxides, hydrochlorination, and elevated reaction temperatures and pressure that are currently used.[3]

Propene (C_3H_6) is a simple HC molecule and an essential feedstock chemical for the synthesis of a large number of important chemicals and polymers.[4,5] Electrochemical oxidation of propene using noble-metal electrodes facilitates generation of a wide variety of products,[6–10] where one of the most promising electrocatalysts reported so far is Pd.[7,11] Electrochemical propene oxidation on Pd leads to the formation of several highly valuable and industrially relevant products such as acrolein, acrylic acid, and propylene glycol. The latter is presumably formed upon hydrolysis of propylene oxide in the electrolyte.[12] The product distribution upon

[a] *Department of Physics, AlbaNova University Center, Stockholm University, 106 91 Stockholm, Sweden. E-mail: sergey.koroidov@fysik.su.se*
[b] *SurfCat, Department of Physics, Technical University of Denmark, Fysikvej, Byg. 311, 2800 Kgs. Lyngby, Denmark*
[c] *Nano-Science Center, Department of Chemistry, University of Copenhagen, Universitetsparken 5, 2100 Copenhagen, Denmark*
† Electronic supplementary information (ESI) available. See DOI: 10.1039/d0cy02134b
‡ Present address: Haldor Topsoe A/S, Haldor Topsøes Allé 1, 2800 Kgs. Lyngby, Denmark.
§ Present address: Carbyon B.V., High Tech Campus 27, 5656 AE Eindhoven, The Netherlands.
¶ Present address: Department of Chemistry – Ångström laboratory, Uppsala University, Box 538, 751 21 Uppsala, Sweden.
|| Present address: SUNCAT Center for Interface Science and Catalysis, SLAC National Accelerator Laboratory, 2575 Sand Hill Road, Menlo Park, CA 94025, United States, and Department of Chemical Engineering, Stanford University, 443 Via Ortega, Stanford, CA 94305, United States.

This journal is © The Royal Society of Chemistry 2021

Catal. Sci. Technol., 2021, **11**, 3347–3352 | **3347**

catalytic propene oxidation depends on which of the unique carbon atoms of propene reacts with an oxygen atom (*e.g.*, provided from H_2O).

Recently, a combined experimental and theoretical study provided a full characterisation of the product distribution in electrochemical propene oxidation as a function of oxidation potential on the Pd electrodes.[12] Using DFT-based reaction modelling, the authors concluded that the reactant coverages on the catalyst surface play a crucial role in determining both the activity and selectivity of the reaction. However, detailed experimental understanding of the surface chemistry during propene oxidation reaction remains elusive. Therefore, the present work aims to characterise *in situ* the changes in the electronic structure of the catalyst that are generated electrochemically during propene oxidation at different electrochemical potentials. We furthermore identify how the surface oxidation influences the selectivity towards reaction with either the allylic carbon or the vinyl group of the propene molecule. In addition, our goal is to probe intermediates and variations in surface coverage to further understand the processes occurring on the Pd electrocatalyst surface under reaction conditions and relate them to the proposed catalytic reaction mechanism.[12] This will in turn provide important information to guide the design for more efficient catalysts.

Results and discussion

In this study, we focus on the anodic propene oxidation on Pd using Pd L_3-edge X-ray absorption spectroscopy (XAS, for experimental details see ESI†) under *operando* conditions. XAS has been used before to examine the electronic structure of catalytic intermediates,[13] as well as to probe catalysts *in situ* in electrochemistry with similar spectral resolution.[14] Due to element specificity and dipole selection rules, the Pd L_3-edge XAS reflects the transition from the Pd $2p_{3/2}$ core level to unoccupied valence orbitals with Pd 4d character. Herein, we exploit that any intermediates formed upon reaction, as well as spectator species adsorbed on the Pd electrode surface, will influence the occupancy of the 4d states of the Pd atoms. Therefore, they affect the Pd L_3-edge intensity, the "white line", and its energy position, which can be used as a sensitive probe of the catalyst state and the chemical processes occurring on the Pd surface under operation.

Before we compare the behaviour of the catalyst in propene and N_2 saturated electrolytes, the electronic structure of the dry Pd nanoparticles dispersed on a conductive carbon support was examined by Pd L_3-edge XAS in a He environment (see Fig. S7†). The energy position of the absorption edge of the dry Pd electrode is observed at 3173.4 eV. The edge shift (+0.4 eV) towards higher energy relative to Pd foil for Pd supported on carbon is well known. This characteristic feature is assigned to metallic Pd(0) nanoparticle size effects and interactions with the carbon

support.[15] The Pd L_3-edge energy in N_2 saturated electrolyte for open circuit potential (OCP) is identical to what is observed for dry Pd nanoparticles (see Fig. S7†). Interaction of N_2 with Pd leads to a substantial Pd L_3-edge shift as well as peak broadening and intensity increase of the white line as has been previously reported in thermocatalysis.[16] Since we have not observed such drastic spectral changes in our experiment, the interaction between Pd and N_2 at the considered experimental conditions can be excluded. Moreover, our theoretical calculations on a Pd(111) model surface suggests that adsorption of neither molecular nor dissociated N_2 is thermodynamically favourable compared to formation of OH(ad) or O(ad) at the relevant potential range of 0.4–1.3 V *vs.* RHE (see below and details in the ESI†).

In situ Pd L_3-edge XAS of Pd in N_2-saturated electrolyte under different electrochemical potentials is shown in Fig. 1A. These spectra establish how the Pd oxidation state changes upon applied electrochemical potential in an inert environment (all potentials in this article are with respect to the reversible hydrogen electrode, RHE). The spectra exhibit a strong dependence on the applied potential. They manifest two transformations: (i) increase of the Pd L_3-edge intensity without appreciable change of the energy position at potentials of up to 1.0 V *vs.* RHE, followed by (ii) continued increase of the white line intensity, accompanied by a change in the Pd L_3-edge peak position at potentials above 1.0 V *vs.* RHE. At any potential, the Pd white line intensity in N_2 saturated electrolyte (Fig. 1A) is higher compared to propene saturated electrolyte (Fig. 1B), where the following spectral changes occur: (i) the Pd L_3-edge (white line) intensity shows almost no potential dependence below 1.1 V *vs.* RHE unlike in N_2, (ii) the change of the Pd L_3-edge intensity in the presence of propene (Fig. 1B) only begins at a potential of 1.1 V *vs.* RHE and the peak position shift towards higher energy is only detected at the highest potential of 1.3 V *vs.* RHE.

In addition to the above, the Pd L_3-edge XAS spectrum of a reference PdO sample collected in He environment is also shown in both Fig. 1A and B. A sharp increase and shift of the white line intensity as well as a different shape in the post edge region is observed compared to the Pd catalyst under all the considered conditions. The increase of the white line intensity in PdO (formally +II) is related to the change in the number of unoccupied valence states containing Pd 4d character. The edge shift towards higher energy for PdO is consistent with the higher effective nuclear charge of Pd in PdO compared to metallic Pd. This result is also in agreement with our reference X-ray photoelectron spectroscopy (XPS) data (Fig. S3†).

In order to elucidate the observed changes on the surface of Pd electrocatalysts in both N_2 and propene saturated electrolytes, we simulated the Pd L_3 XAS spectra using *ab initio* multiple scattering calculations FEFF 9.6.4 (ref. 17) based on model structures of the catalyst (see multiple-scattering calculations section in ESI†). The calculated Pd L_3-edge XAS spectra (Fig. 1C) are in good qualitative agreement with the experimental results (Fig. 1A and B). The calculated
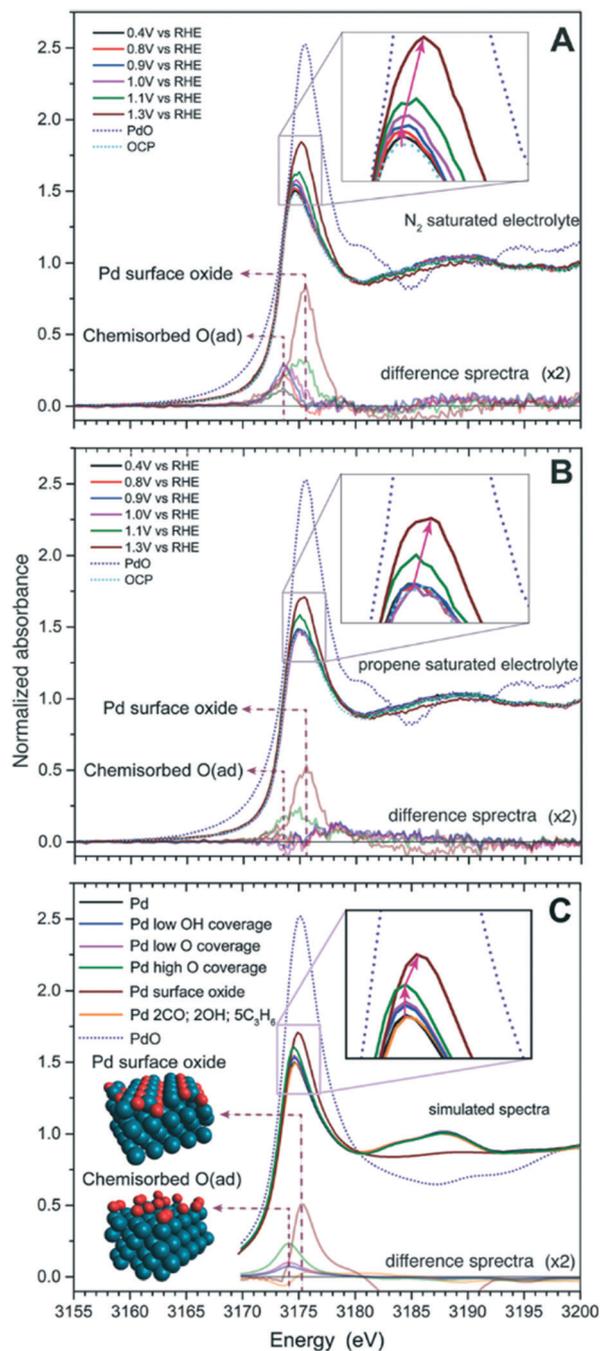
Fig. 1 Pd L_3-edge XAS spectra of Pd electrocatalysts recorded *in situ* in H_3PO_4/NaH_2PO_4 electrolyte, pH 2.8, saturated with (A) N_2 and (B) propene; (C) simulated XAS spectra using FEFF 9.6.4. The structure of chemisorbed O(ad) corresponds to Pd high O coverage; (difference spectra; A, B and C) relative changes in formation of the two different oxygen species (Pd surface oxide and chemisorbed O(ad)) on the Pd electrode surface upon applied electrochemical potential relative open circuit potential (OCP). Changes in the Pd L_3-edge are illustrated using the same colour code as the applied electrochemical potential. For better representation, the difference spectra are multiplied by 2; insets in all figures have identical magnification and illustrate overall evolution of the Pd white line intensity as a function of the applied oxidation potential.

spectra show that the amount of chemisorbed O(ad)/OH(ad) is expected to gradually increase the Pd L_3-edge intensity without changing the edge position. These results (Fig. 1) are qualitatively well in line with previous work on Pt where the potential dependence of chemisorbed O(ad)/OH(ad) and platinum oxide formation was studied using Pt L_3-edge XAS.[14] Both OH(ad) and O(ad) are predicted to have the same effect on the Pd L_3 edge intensity (Fig. 1C; Pd low O/OH coverage). Thus, spectral changes seen upon increasing the potential from +0.4 V to +1.0 V *vs.* RHE in N_2 saturated electrolyte and at +1.1 V *vs.* RHE in propene saturated electrolyte are consistent with chemisorbed OH(ad)/O(ad) being formed on the metallic Pd surface (see structure in Fig. 1C). This agrees well with several previous electrochemical studies carried out in a similar pH range and potential window,[18–20] which show that the Pd electrode surface is mostly covered by OH(ad) and O(ad) species.

In addition to the FEFF calculations, our electrochemical simulations using DFT in combination with the generalised computational hydrogen electrode (GCHE)[21] method shed further light on the interface of Pd with adsorbates. On Pd(111) with N_2 added as possible adsorbate, we find OH(ad) to be prevalent in the range of 0.4 to ~1.0 V *vs.* RHE, see simulated interface prevalence diagram in Fig. 2A. At potentials >1.0 V *vs.* RHE, O(ad) replaces OH(ad) on the clean Pd surface, before PdO becomes the most stable state at approximately 1.1 V *vs.* RHE. This is, thus, in close agreement with the changes observed in the Pd L_3-edge XAS spectra in nitrogen-saturated electrolyte, with minor spectral changes below 1.0 V *vs.* RHE corresponding to the gradually increasing surface oxidation going from OH(ad) to O(ad), tentatively followed by formation of a thicker oxide layer associated with a larger spectral response.

The surface characteristics change under exposure to propene. Several previous studies reported the formation of palladium carbides (Pd–C) during thermal hydrogenation of alkynes.[22,23] Indeed, our theoretical simulations suggest that atomic carbon is stable on the Pd surface with respect to propene (Fig. 2B), but unstable compared to possible oxidation products, such as CO(ad) and subsequently formed $CO_2(g)$ at oxidising potentials. A full microkinetic model that could resolve this is beyond the scope of this paper, however, further insight into the surface state can be gained from our XAS data. It is known that the formation of Pd–C results in a 5 eV shift of the Pd L_3-edge towards higher energy compared to metallic Pd and also leads to a decrease of the white line intensity.[24] Neither of these effects can be seen in the spectra obtained in the present study (Fig. 1). This suggests that the Pd–C coverage is low under operational conditions and will not influence the electrocatalytic propene oxidation to any significant degree.

The above also finds support from theory. While a full analysis of the steady-state surface coverage on the Pd catalyst requires knowledge of the energetics and barriers for all processes taking place on the surface, which is beyond the scope of the present study, our computations together with
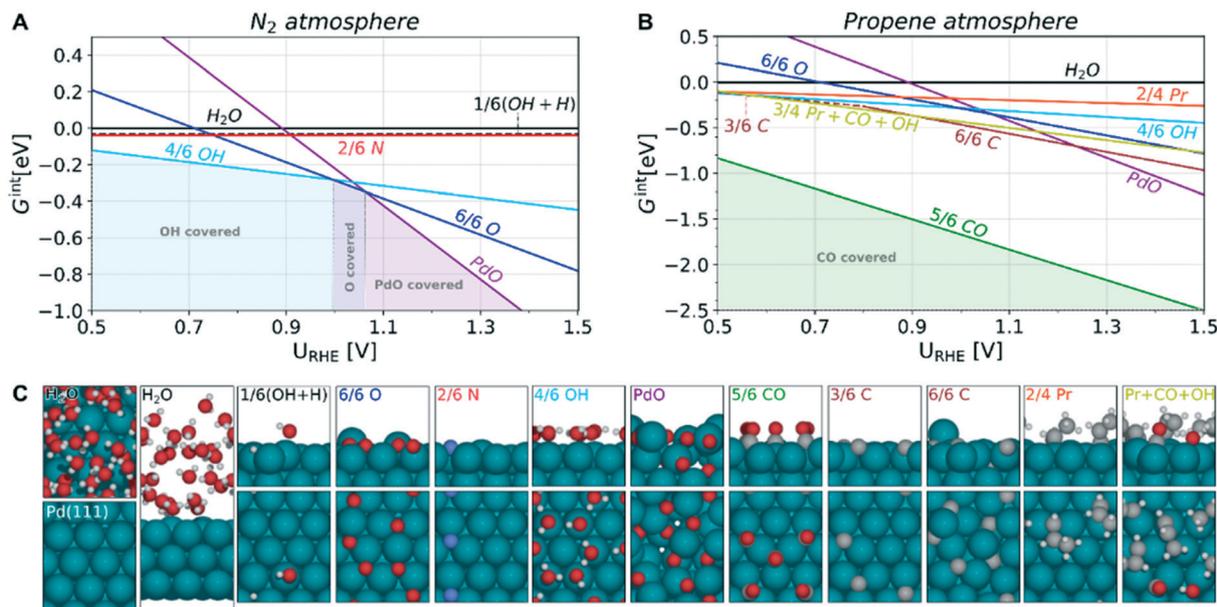
This journal is © The Royal Society of Chemistry 2021

Catal. Sci. Technol., 2021, **11**, 3347–3352 | **3349**

Fig. 2 Simulated phase diagrams for Pd(111) at pH 2.8 in 1 bar A) nitrogen, and B) propene atmosphere, respectively, using the GCHE-DFT method.[21,27,28] Only the most favorable surface coverage is included for each adsorbate. See ESI† for full data and description of the methods. In C), the low-energy structures of each adsorbate state are shown. H_2O molecules are omitted for visibility, except for the H_2O reference state and highly H-bonded OH* state, for which H_2O in the first adsorption layer are shown. Color code atomic model: Pd (teal), O (red), H (white), N (blue), C (grey).
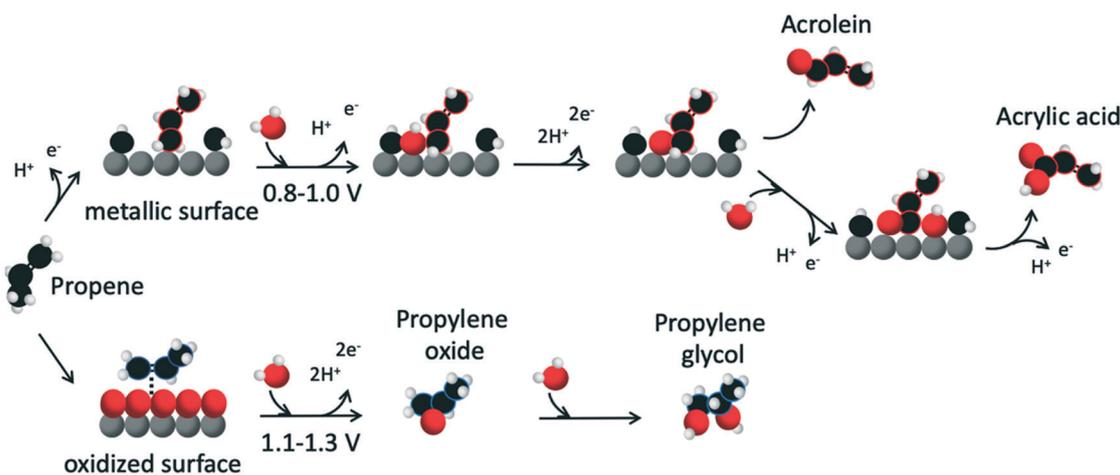

Fig. 3 Possible reaction mechanisms of propene oxidation. The mechanisms are built on our *in situ* probing of the Pd catalyst surface and previous suggestions by Winiwarter *et al.*,[12] as well as DFT simulations (Fig. S8 and S11†). Palladium, grey; carbon, black; oxygen, red; hydrogen, white.

the results of a previous study[12] offer some insight. We first note that in order to form Pd–C (a six-electron process), it needs to compete with less demanding two-electron oxidation reactions (leading to *e.g.* acrolein and propylene oxide) as well as with ultrathin PdO formation – the latter causing spectral shape changes as discussed above. The barrier for further oxidation of C to CO/CO_2 must also be sufficiently high to allow for the build-up of Pd–C at the surface. Accounting for all of these processes, Winiwarter *et al.* have suggested that under reaction conditions the Pd surface is covered by different types of deprotonated propene, with

competition from OH. This adsorbate competition is in fact believed to be beneficial for the selective formation of acrolein and acrylic acid from propene. Our simulations show that a mixed propene/CO/OH state is more stable than, or of similar stability as, surface Pd–C over the potential range of 0.4 to 1.0 V *vs.* RHE. It was also suggested,[12] that a surface largely covered by CO would be very stable. However, a high CO-coverage is not supported by our experimental results, since the associated spectral changes are not observed (see simulated XAS spectra in Fig. S10†) and would likely also result in a different cyclic voltammogram than the

3350 | *Catal. Sci. Technol.*, 2021, **11**, 3347–3352

This journal is © The Royal Society of Chemistry 2021

one observed in propene.[12] It is known that CO is readily oxidized to CO_2 on Pd at potentials around and above 0.85 V vs. RHE,[12,25] which we believe is a key reason for the lack of CO features in the measured XAS spectra.

The signature of Pd–OH(ad)/O(ad) species in the potential range of 0.4–1.0 V vs. RHE is only visible in the Pd L_3-edge XAS spectra for the Pd electrode in the N_2 saturated electrolyte (Fig. 1A). For the propene saturated electrolyte (Fig. 1B; 0.4–1.0 V vs. RHE) and the simulated spectra of Pd surface covered by propene, CO and OH (Fig. 1C; Pd 2CO, 2OH, $5C_3H_6$), no such signature is present in this potential region. This lack of characteristic OH(ad)/O(ad) features suggests that the chemisorbed propene suppresses the surface coverage of oxygen-containing species, which leads to higher onset potential for the adsorption of OH(ad)/O(ad), consequently leading to a higher propene vs. OH(ad)/O(ad) coverage ratio. Cyclic voltammetry strongly supports this interpretation (Fig. S4†). If the potential is scanned up to 1.3 V vs. RHE, where the Pd surface is highly oxidised,[19,20] the intensity of the reduction peak in the cathodic scan, which is proportional to the amount of oxide formed on the Pd surface, has a more prominent feature in N_2-saturated electrolyte compared to the propene-saturated electrolyte (see Fig. S4†). Further support of higher oxidation of the Pd surface in N_2-saturated electrolyte is found from comparing the intensity of the Pd L_3-edge and difference spectra for the highest potential for both electrolytes (Fig. 1A and B). Again this is in agreement with our DFT simulations that suggest that propene or propene-derived intermediates suppress OH(ad)/O(ad) at the Pd interface (Fig. 2). Since propene adsorption is thermodynamically more favourable than the formation of OH(ad)/O(ad) species, which are required for the catalytic reaction, we conclude that their surface adsorption (OH(ad)/O(ad)) is likely to become the rate-limiting factor for the propene oxidation reaction towards acrolein and acrylic acid.

Our XPS measurements of the Pd 2p-region show that formation of thin Pd surface oxide on metallic Pd leads to the appearance of an additional component that causes the formation of a shoulder on the high binding energy side (Fig. S3†). This is consistent with the white line shift in the XAS spectra (Fig. 1A and B) at higher potentials. However, since the Pd L_3-edge intensity for the highest potential in propene- and N_2-saturated electrolytes has a significantly lower intensity and is less broad than in both the measured (Fig. 1A and B) and simulated (Fig. 1C) bulk PdO, the formation of a thick layer of palladium oxide can be excluded in our experiment. To identify the fingerprint of an ultrathin surface oxide that grows on the metallic Pd surface at an increased electrochemical potential above 1.0 V in N_2 and at 1.3 V in propene (Fig. 1A and B), we assume that its short-range structure resembles the well-known structure of bulk PdO.[26] Thus, the calculated spectrum of PdO is used as a first approximation to identify the features of an ultrathin surface oxide (Fig. 1C). On the other hand, simulated spectra of ultrathin surface oxide (Fig. 1C; Pd surface oxide) yield a

computed intensity closely matching the measurements at 1.3 V (Fig. 1B), which supports that surface-oxide formation causes the broadening and the Pd L_3-edge position shift.

Under the experimental conditions used in the present study, Pd has previously been shown to exhibit catalytic activity for propene oxidation towards different (valuable) products as a function of the applied potential. The production rates of acrolein and acrylic acid are the highest at 0.9 V, while propylene glycol generation becomes significant at 1.1 V and its partial current density and faradaic efficiency increase with higher anodic potentials.[12] Also, it was found that the onset of propene oxidation at 0.7 V overlaps with water activation; the adsorption energy of propene is more exergonic compared to OH(ad)/O(ad). The Pd L_3 edge spectra (Fig. 1B) show that in the presence of propene, the amount of chemisorbed oxygen species is reduced in the potential range between 0.4–1.0 V vs. RHE in comparison to the spectra in N_2 saturated electrolyte. This suggests that electrochemically induced surface coverage of OH(ad)/O(ad) on the Pd electrode is low during the catalytic oxidation of propene to acrolein and acrylic acid (Fig. 1C; Pd 2CO, 2OH, $5C_3H_6$), which is further supported by our DFT simulations of the Pd interface under different conditions. Propene activation in the allylic position is consistent with acrolein and acrylic acid formation: upon adsorption on Pd, the allylic carbon of propene deprotonates and reacts with adsorbed OH(ad)/O(ad) (Fig. 2). In contrast, reaction via the Eley–Rideal type mechanism, where OH/H_2O reacts with the absorbed propene molecule directly from the liquid phase, is not in line with the product distribution of propene oxidation on Pd for the potential range between 0.4–1.0 V vs. RHE as this would most probably go through reaction with the vinyl group. Additionally, propene adsorption through the vinyl group on metallic Pd would lead to irreversibly retained, unreactive adsorbates such as C_2H_x, CH_y. These species are highly stable and do not react further resulting in a high surface coverage of these species that can be stripped off as CO_2 only at high anodic potential.[12,25,29] Therefore, we argue that our results provide experimental support for a Langmuir–Hinshelwood mechanism as the dominant path leading to acrolein and acrylic acid formation, which agrees with the reaction mechanism previously suggested by Winiwarter et al.[12] For the potential range between 1.1–1.3 V vs. RHE, on the other hand, where propylene glycol is formed, we observe surface oxide growth (Fig. 1B). While we are not able to conclusively resolve the 1.1–1.3 V vs. RHE mechanism, we propose from the above that propene oxidation towards propylene oxide, which requires oxidation of the vinyl group, can only occur on an oxidised Pd surface (Fig. 3). As the propylene oxide intermediate spontaneously desorbs and dissolves in the aqueous solution (see Fig. S11†), we also suggest that propylene glycol is thereafter formed in solution by acid catalysed hydrolysis as propylene oxide is not stable in aqueous environment.[4]

This journal is © The Royal Society of Chemistry 2021

Catal. Sci. Technol., 2021, **11**, 3347–3352 | **3351**

Conclusions

In summary, based on our results and the previous study by Winiwarter et al.,[12] we propose two different mechanisms of the propene oxidation reaction that depend on the applied potential as illustrated in Fig. 3. Selective allylic oxidation of propene to acrolein and acrylic acid occurs on the metallic Pd surface via the Langmuir–Hinshelwood mechanism in the potential range of 0.8–1.0 V vs. RHE while for the potential range, 1.1–1.3 V vs. RHE, selective oxidation of the vinyl group to propylene glycol takes place on the Pd oxide surface.

This work shows the impact the formation of surface oxide on the catalyst has on the selectivity and reactivity towards different products. The information obtained in this study provides guidance for tailoring new catalysts by tuning carbophilic or oxophilic properties of the catalyst, for selective generation of different high-value target chemicals from less toxic reactants than today's common production methods and with improved selectivity, leading to the reduction of chemical waste.

Conflicts of interest

There are no conflicts to declare.

Acknowledgements

References

1 J. Warnatz, Ber. Bunsenges. Phys. Chem., 1983, 87, 1008–1022.

2 J. Haber, Handb. Heterog. Catal., 2008, 3359–3384.

3 T. A. Nijhuis, M. Makkee, J. A. Moulijn and B. M. Weckhuysen, Ind. Eng. Chem. Res., 2006, 45, 3447–3459.

4 S. J. Khatib and S. T. Oyama, Catal. Rev.: Sci. Eng., 2015, 57, 306–344.

5 P. Sprenger, W. Kleist and J.-D. Grunwaldt, ACS Catal., 2017, 7, 5628–5642.

6 C. Tse-Chuan and C. Jang-Chyang, Chem. Eng. Sci., 1980, 35, 1581–1590.

7 K. Otsuka, Y. Shimizu, I. Yamanaka and T. Komatsu, Catal. Lett., 1989, 3, 365–369.

8 F. Goodridge, S. Harrison and R. E. Plimley, J. Electroanal. Chem. Interfacial Electrochem., 1986, 214, 283–293.

9 V. M. Schmidt and E. Pastor, J. Electroanal. Chem., 1996, 401, 155–161.

10 M. Bełtowska-Brzezinska, T. Łuczak, H. Baltruschat and U. Müller, J. Phys. Chem. B, 2003, 107, 4793–4800.

11 G. R. Stafford, Electrochim. Acta, 1987, 32, 1137–1143.

12 A. Winiwarter, L. Silvioli, S. B. Scott, K. Enemark-Rasmussen, M. Sariç, D. B. Trimarco, P. C. K. Vesborg, P. G. Moses, I. E. L. Stephens, B. Seger, J. Rossmeisl and I. Chorkendorff, Energy Environ. Sci., 2019, 12, 1055–1067.

13 S. Koroidov, K. Hong, K. S. Kjaer, L. Li, K. Kunnus, M. Reinhard, R. W. Hartsock, D. Amit, R. Eisenberg and C. Das Pemmaraju, Inorg. Chem., 2018, 57, 13167–13175.

14 D. Friebel, V. Viswanathan, D. J. Miller, T. Anniyev, H. Ogasawara, A. H. Larsen, C. P. Ogrady, J. K. Nørskov and A. Nilsson, J. Am. Chem. Soc., 2012, 134, 9664–9671.

15 E. O. Pentsak, A. S. Kashin, M. V. Polynski, K. O. Kvashnina, P. Glatzel and V. P. Ananikov, Chem. Sci., 2015, 6, 3302–3313.

16 E. K. Dann, E. K. Gibson, R. H. Blackmore, C. R. A. Catlow, P. Collier, A. Chutia, T. E. Erden, C. Hardacre, A. Kroner, M. Nachtegaal, A. Raj, S. M. Rogers, S. F. R. Taylor, P. Thompson, G. F. Tierney, C. D. Zeinalipour-Yazdi, A. Goguet and P. P. Wells, Nat. Catal., 2019, 2, 157–163.

17 J. J. Rehr, J. J. Kas, F. D. Vila, M. P. Prange and K. Jorissen, Phys. Chem. Chem. Phys., 2010, 12, 5503–5513.

18 A. E. Bolzán, M. E. Martins and A. J. Arvía, J. Electroanal. Chem. Interfacial Electrochem., 1984, 172, 221–233.

19 A. Bolzan, M. E. Martins and A. J. Arvia, J. Electroanal. Chem. Interfacial Electrochem., 1986, 207, 279–292.

20 X. Chen, L. P. Granda-Marulanda, I. T. McCrum and M. T. M. Koper, Chem. Sci., 2020, 11, 1703–1713.

21 J. Rossmeisl, K. Chan, R. Ahmed, V. Tripković and M. E. Björketun, Phys. Chem. Chem. Phys., 2013, 15, 10321–10325.

22 M. W. Tew, M. Nachtegaal, M. Janousch, T. Huthwelker and J. A. van Bokhoven, Phys. Chem. Chem. Phys., 2012, 14, 5761–5768.

23 A. L. Bugaev, A. A. Guda, I. A. Pankin, E. Groppo, R. Pellegrini, A. Longo, A. V. Soldatov and C. Lamberti, Data in Brief, 2019, 24, 103954.

24 M. W. Tew, M. Janousch, T. Huthwelker and J. A. van Bokhoven, J. Catal., 2011, 283, 45–54.

25 T. Mittermeier, A. Weiß, H. A. Gasteiger and F. Hasché, J. Electrochem. Soc., 2017, 164, F1081–F1089.

26 J. Waser, H. A. Levy and S. W. Peterson, Acta Crystallogr., 1953, 6, 661–663.

27 J. H. Stenlid, E. Campos dos Santos, R. M. Arán Ais, A. Bagger, A. J. Johansson, B. R. Cuenya, J. Rossmeisl and L. G. M. Pettersson, Electrochim. Acta, 2020, 137111.

28 J. H. Stenlid, E. C. Dos Santos, A. Bagger, A. J. Johansson, J. Rossmeisl and L. G. M. Pettersson, J. Phys. Chem. C, 2020, 124, 469–481.

29 A. Winiwarter, M. J. Boyd, S. B. Scott, D. C. Higgins, B. Seger, I. Chorkendorff and T. F. Jaramillo, ChemElectroChem, 2021, 8(1), 250–256.

3352 | Catal. Sci. Technol., 2021, 11, 3347–3352

This journal is © The Royal Society of Chemistry 2021